IEEE Access
Multidisciplinary | Rapid Review | Open Access Journal

Received June 8, 2018, accepted July 3, 2018, date of publication July 9, 2018, date of current version August 7, 2018.

Digital Object Identifier 10.1109/ACCESS.2018.2854307

Spatial Separation of Closely-Located Users in Measured Massive MIMO Channels

JOSE FLORDELIS[1], (Student Member, IEEE), FREDRIK RUSEK[1], (Member, IEEE), XIANG GAO[2], GHASSAN DAHMAN[3], (Member, IEEE), OVE EDFORS[1], (Senior Member, IEEE), AND FREDRIK TUFVESSON[1], (Fellow, IEEE)

[1]Department of Electrical and Information Technology, Lund University, SE-221 00 Lund, Sweden
[2]National Key Laboratory of Science and Technology on Communications, University of Electronic Science and Technology of China, Chengdu 611731, China
[3]École de Technologie Supérieure, Montreal, QC H3C 1K3, Canada

Corresponding author: Jose Flordelis (jose.flordelis@eit.lth.se)

This work was supported in part by the Seventh Framework Programme (FP7) of the European Union (MAMMOET), ELLIIT—an Excellence Center, Linköping-Lund in Information Technology, under Grant 619086, in part by the Swedish Research Council (VR), and in part by the Swedish Foundation for Strategic Research (SSF).

ABSTRACT We investigate the ability of Massive multiple-input multiple-output (MIMO) systems to spatially separate up to eighteen users located close to one another in line-of-sight (LOS) propagation conditions, in both indoor and outdoor environments. For that, we use fully-synchronous measured channels at 2.6 GHz of single-antenna users moving within a small area and concurrently communicating with a base station (BS) equipped with a compact 128-port array. To quantify the degree of spatial user separability, we use three scalar metrics, namely, the achievable sum-rates, the condition number of the channel matrix, and the angle to interference factor. Our results show that Massive MIMO with zero-forcing (ZF) or regularized ZF (RZF) can spatially separate nine, even eighteen, concurrent users at practical SNR values even in the challenging case of dominant LOS propagation. In particular, signal-to-noise ratio losses relative to ideal (non-interfering and equally strong) channels can be reduced dramatically compared with standard multiuser MIMO systems, which typically have the same number of users as BS antennas. Our findings suggest that with RZF or ZF the ratio of BS antennas to number of served users should be at least three to four, to harvest most of the available spatial gains that the environment can offer. Although orthogonality and array gains complement each other, for the suggested ratios of antennas to users, the main contribution to improving system performance, measured in sum-rates, comes from the orthogonality gain.

INDEX TERMS Channel measurements, Massive MIMO, spatial separation.

I. INTRODUCTION

Massive multiple-input multiple-output (MIMO) promises orders-of-magnitude improvements in data throughput and transmit-energy efficiency while using low-complexity linear precoding and decoding schemes [1]–[5]. These benefits arise from leveraging the spatial degrees of freedom of an excess of antennas at the base station (BS). Typically, a BS equipped with many antennas, say $M = 100$, serves K single-antenna users in the same time-frequency resource, with $\frac{M}{K} \gg 1$. Due to the potential to greatly increase spectral efficiency compared to today's systems, Massive MIMO is considered a main candidate for next-generation wireless systems [6]–[8].

The concept has since its inception [9] advanced rapidly from theory to practice. Information-theoretic analyses have been developed [5], experiments in real propagation environments have validated theoretical predictions [10]–[12], and test beds have confirmed the feasibility of practical implementations [13]. However, uncertainty remains, e.g., regarding the performance of Massive MIMO in some propagation scenarios particularly difficult for spatially multiplexing users. Two such scenarios, identified [14], [15] as important for future 5G systems, are 1) "open exhibition", addressing outdoor activities such as live concerts or sport events where a crowd gathers, and 2) "crowded auditorium", focusing on indoor concert halls and conference venues. In both scenarios, a large number of users with limited mobility are located physically close to one another, often with line-of-sight (LOS) to the BS. Dominant LOS propagation with closely-located users is challenging because signals arrive at

the BS mostly from one direction. Thus, one key aspect to analyze is the ability of the Massive MIMO BS to spatially separate signals received from, or transmitted to, a crowd of users. Note that current communication standards such as LTE [16] and IEEE 802.11 WLAN [17], in which the number of BS antennas is typically the same as the total number of user antennas, have difficulties with spatial multiplexing of users in the above scenarios.

Simply put, the main question addressed in this paper is: ''Can Massive MIMO with practical precoding schemes spatially separate a group of users located close to one another?'' To answer this question, we conducted fully-synchronous channel measurements of groups of nine users in both indoor and outdoor environments at 2.6 GHz, and analyze the performance of zero-forcing (ZF) and regularized ZF (RZF) transmission—we showed in [11] that maximum ratio transmission (MRT) does not work well with closely-located users in LOS. Crucially, our measurements include the effect of the users' hands, bodies and antennas, for a realistic performance assessment.

In [18]–[20], we reported outdoor Massive MIMO channel measurements, whereas indoor measurements were reported in [21] (see also [22], [23]). All these investigations rely on the notion of ''virtual'' users and arrays, meaning that user channels are obtained by selecting data from measurements at different positions or time instants. Although technically straightforward, measurements obtained in this fashion suffer from some inherent limitations. Specifically, such measurements do not capture the time-variant properties of the channel. To date, fully-synchronous measurements with ''real'' users and arrays have been reported in [24] (indoor), [11] (outdoor), and [25]. While [24] and [25] focus on important properties of the Massive MIMO channel such as the channel condition number and the user orthogonality, these investigations omit direct metrics of system performance, notably the achievable sum-rates.

The key contributions of the paper at hand are the following:

- Based on fully-synchronous measured channels, we show that nine, even eighteen, concurrent, closely-located users can be separated with RZF or ZF and Massive MIMO using a compact array in the difficult scenario of dominant LOS propagation, both indoors and outdoors.
- We quantify the amount of BS antennas that are required to spatially separate concurrent users. Our findings suggest that three to four times as many antennas as active users is sufficient.
- We show that the main contribution to improving system performance comes from the orthogonality gain of Massive MIMO, although in general the orthogonality gain and the array gain complement each other.
- We use the angle to interference factor, which we shall precisely define later on, as a metric of spatial user separability, and show that it can be directly linked to the performance of ZF. We also provide novel expressions relating the smallest singular value of multiuser (MU) MIMO channels with the performance of ZF.

Notation: Throughout the paper, boldface lowercase $\mathbf{a}$ represent column vectors, and boldface uppercase $\mathbf{A}$ matrices. The symbol $\mathbf{I}$ denotes the identity matrix. Using this notation, $\mathrm{tr}\,(\mathbf{A})$ is the trace, $\mathbf{A}^{\mathrm{T}}$ the transpose, $\mathbf{A}^{*}$ the conjugate, $\mathbf{A}^{\mathrm{H}}$ the Hermitian transpose, $|\mathbf{A}|$ the determinant, $\left[\mathbf{A}\right]_{ij}$ the $(i,j)^{\mathrm{th}}$ element of $\mathbf{A}$, and $\mathbf{A} \succeq \mathbf{0}$ means that $\mathbf{A}$ is positive semidefinite. Furthermore, $\|\mathbf{a}\|$ is the Euclidean norm, $\mathrm{diag}(\mathbf{a})$ a matrix having $\mathbf{a}$ along its diagonal and zeros elsewhere, $\mathcal{CN}(\mathbf{a}, \mathbf{A})$ the complex Gaussian distribution with mean $\mathbf{a}$ and covariance matrix $\mathbf{A}$, and $\mathbf{E}\{\cdot\}$ the expectation operator.

II. SIGNAL MODEL

We consider the downlink (DL) of a MU-MIMO system. In this system, an M-antenna BS communicates with K single-antenna users, where $K \leq M$. Orthogonal frequency division multiplexing (OFDM) [26] with L subcarriers is assumed. Let $\mathbf{h}_i(\ell, n) \in \mathbb{C}^{M\times 1}$ denote the channel vector between the BS and the i^{th} user during the ℓ^{th} OFDM subcarrier ($\ell = 1, \ldots, L$) and n^{th} OFDM symbol ($n = 1, 2 \ldots, N$). Vectors $\mathbf{h}_i(\ell, n)$ are obtained through channel measurements with an antenna array, and include the effects of small- and large-scale fading, and shadowing by users [27]. We treat them as vector-valued random variables and normalize them so that the average channel gain, $\mathbf{E}\{\|\mathbf{h}_k(\ell, n)\|^2\}$, is M, for $k = 1, \ldots, K$. If $\mathbf{H}(\ell, n) = \left[\mathbf{h}_1(\ell, n) \cdots \mathbf{h}_K(\ell, n)\right]^{\mathrm{T}}$ denotes the MU-MIMO channel matrix, then the baseband complex representation of the received signal vector is

$$\mathbf{y}(\ell, n) = \mathbf{H}(\ell, n)\,\mathbf{s}(\ell, n) + \mathbf{n}(\ell, n), \tag{1}$$

where $\mathbf{s}(\ell, n) \in \mathbb{C}^{M\times 1}$ is the transmitted signal vector with $\mathbf{E}\left\{\mathbf{s}^{\mathrm{H}}(\ell, n)\mathbf{s}(\ell, n)\right\} = E_{\mathrm{s}}$, where $E_{\mathrm{s}} > 0$ is the average energy available at the BS per time-frequency resource, and $\mathbf{n}(\ell, n)$ the vector of receiver noise with independent identically distributed (iid) $\mathcal{CN}(0, N_0)$ entries. We define the signal-to-noise ratio (SNR) as $\rho = \frac{E_{\mathrm{s}}}{N_0}$. Throughout this work, we assume that each channel realization $\mathbf{H}(\ell, n)$ is fixed and known perfectly to both the BS and the users (i.e., having full channel state information (CSI)). For the sake of simplicity we drop indexes ℓ and n in much of the rest of the paper since signal processing is mainly done per time-frequency resource.

III. METRICS OF SPATIAL USER SEPARABILITY

We devote this section to reviewing various metrics of spatial user separability, which we will later use in Sec. V.

A. SUM-RATES

Cellular systems are often compared and evaluated by the sum-rates they support. In this work, we consider three sum-rate metrics. The first one is the sum-capacity of MU-MIMO channels [28]–[31], known to be achievable by dirty-paper coding (DPC) [32]. Under the full CSI assumption above, the sum-capacity of a given (ℓ, n)-th time-frequency resource,

$\mathcal{C}_{\mathrm{DPC}}(\mathbf{H}, \rho)$, in bps/Hz, can be found as the solution to [2]

$$\begin{aligned} \underset{\mathbf{\Lambda}}{\text{maximize}} \quad & \log_2 \left| \mathbf{I} + \rho\, \mathbf{H}^{\mathrm{H}} \mathbf{\Lambda} \mathbf{H} \right| \\ \text{subject to} \quad & \mathrm{tr}\,(\mathbf{\Lambda}) = 1, \quad \mathbf{\Lambda} \succeq 0, \end{aligned} \tag{2}$$

where $\mathbf{\Lambda} = \mathrm{diag}(\lambda_1, \ldots, \lambda_K)$ is a diagonal power-loading matrix. Problem (2) is convex and can be solved efficiently via a technique known as sum-power iterative waterfilling [33], [34]. The sum-capacity averaged over all the time-frequency resources is then

$$\bar{\mathcal{C}}_{\mathrm{DPC}}(\rho) = \frac{1}{LN} \sum_{n=1}^{N} \sum_{\ell=1}^{L} \mathcal{C}_{\mathrm{DPC}}(\mathbf{H}(\ell, n), \rho). \tag{3}$$

Unfortunately, DPC is known to be computationally very intensive and therefore not suitable for practical deployments.

Because of their low computational complexity, linear precoding schemes constitute a popular alternative to DPC. Moreover, it is shown in [1] that under asymptotically favorable propagation (i.e., $\lim_{M\to\infty} \mathbf{h}_i^{\mathrm{H}} \mathbf{h}_j / (\|\mathbf{h}_i\| \cdot \|\mathbf{h}_j\|) = 0, i \neq j$), certain linear precoding schemes approach the sum-capacity as $M \to \infty$. For the second sum-rate metric, we consider the sum-rate $\mathcal{C}_{\mathrm{ZF}}(\mathbf{H}, \rho)$ of the ZF precoder [35], [36], given by the solution to:

$$\begin{aligned} \underset{\mathbf{\Lambda}}{\text{maximize}} \quad & \sum_{k=1}^{K} \log_2 \left(1 + \rho\, \lambda_k g_k^2 \right) \\ \text{subject to} \quad & \mathrm{tr}\,(\mathbf{\Lambda}) = 1, \quad \mathbf{\Lambda} \succeq 0, \end{aligned} \tag{4}$$

where $g_k^2 = 1 / \left[(\mathbf{H}\mathbf{H}^{\mathrm{H}})^{-1} \right]_{kk}$, and $\mathbf{H}$ is assumed full-rank. Problem (4) can be readily solved by waterfilling [37] on the quantities $\{g_k^2\}_{k=1}^K$. The ZF sum-rate averaged over all time-frequency resources, $\bar{\mathcal{C}}_{\mathrm{ZF}}(\rho)$, is then defined similar to (3). Among the class of linear precoding schemes, RZF precoding is often preferred in practical MIMO deployments due to its reliability and good performance [38], and hence we consider it for the third sum-rate metric. For each time-frequency resource, we compute the sum-rate $\mathcal{C}_{\mathrm{RZF}}(\mathbf{H}, \rho)$ as the solution to:

$$\begin{aligned} \underset{\mathbf{\Lambda}}{\text{maximize}} \quad & \sum_{k=1}^{K} \log_2 \left(1 + \frac{\frac{\rho}{M} \lambda_k |\mathbf{h}_k^{\mathrm{H}} \mathbf{w}_k|^2}{\sum_{i \neq k} \frac{\rho}{M} \lambda_k |\mathbf{h}_k^{\mathrm{H}} \mathbf{w}_i|^2 + 1} \right) \\ \text{subject to} \quad & \mathrm{tr}\,(\mathbf{\Lambda}) = 1, \quad \mathbf{\Lambda} \succeq 0, \end{aligned} \tag{5}$$

where $\mathbf{w}_k$ is the k^{th} column of the precoding matrix $\mathbf{W} = \mathbf{H}^{\mathrm{H}} \left(\mathbf{I} + \frac{\rho}{K} \mathbf{H}\mathbf{H}^{\mathrm{H}} \right)^{-1}$ normalized to have unit norm. The RZF sum-rate averaged over all time-frequency resources, $\bar{\mathcal{C}}_{\mathrm{RZF}}(\rho)$, is then defined similar to (3). As for MRT, we showed in [11] that this precoding scheme does not separate closely-located users well in LOS propagation conditions, and therefore we do not consider it in the present work.

B. CHANNEL CONDITION NUMBER

The channel condition number is often used as an indication of the degree of mutual orthogonality among users' channels [5], [10]. With $\sigma_1 \geq \ldots \geq \sigma_K \geq 0$ being the ordered singular values of $\mathbf{H} = \left[\mathbf{h}_1 \cdots \mathbf{h}_K \right]^{\mathrm{T}}$,[1] we define the condition number

$$\kappa = \frac{\sigma_1}{\sigma_K}, \tag{6}$$

and its dB value $\kappa_{\mathrm{dB}} = 20 \log_{10} \kappa$. Clearly, $1 \leq \kappa \leq \infty$. From the viewpoint of spatial user separability, one desires κ close to one. In particular, if $\kappa = 1$ we have favorable propagation [5] even at finite M (that is, $\mathbf{h}_i^{\mathrm{H}} \mathbf{h}_j = 0, i \neq j$).[2] In general, for fixed transmit energy E_{s}, achievable sum-rates decrease with increasing κ. We will see later in Sec. V, however, that although there is a loss relative to favorable propagation, satisfactory sum-rates may still be extracted for not-so-large values of κ. Hence, except for κ close to one, the relationship between channel condition number and achievable sum-rates is somewhat loose, and κ should be considered only as a coarse indication of system performance.

C. ANGLE TO INTERFERENCE SUBSPACE

To partly overcome the limitations of the channel condition number κ, we propose a third metric of spatial user separability, namely the angle

$$\theta_k = \cos^{-1} \left(\frac{\|\mathbf{P}_k \mathbf{h}_k\|}{\|\mathbf{h}_k\|} \right), \quad k = 1, \ldots, K, \tag{7}$$

between the user channel $\mathbf{h}_k$ and the subspace spanned by the rows of $\mathbf{H}_{(k)} = \left[\mathbf{h}_1 \ldots \mathbf{h}_{k-1}\, \mathbf{h}_{k+1} \ldots \mathbf{h}_K \right]^{\mathrm{T}}$, which contains the interfering user channels. Here, $\mathbf{P}_k = \mathbf{H}_{(k)}^{\mathrm{T}} (\mathbf{H}_{(k)}^{*} \mathbf{H}_{(k)}^{\mathrm{T}})^{-1} \mathbf{H}_{(k)}^{*}$ is the orthogonal projection matrix of $\mathbf{h}_k$ onto $\mathbf{H}_{(k)}^{\mathrm{T}}$. For our purposes, it is convenient to restrict θ_k to the interval $[0, \pi]$. By a brief calculation, one can rewrite (7) as

$$\sin^2 \theta_k = g_k^2 / \|\mathbf{h}_k\|^2, \quad k = 1, \ldots, K. \tag{8}$$

We call $\xi_k = \sin^2 \theta_k$ the angle to interference *factor*, and note that the condition $\xi_k = 1$, for $k = 1, \ldots, K$, is equivalent to favorable propagation. Furthermore, it can be shown that the angle to interference factor ξ_k represents the fraction of the channel gain $\|\mathbf{h}_k\|^2$ that is available for communication when using ZF. Because of this, ξ_k can be directly related to system performance. In fact, for the case in question of closely-located users in LOS propagation conditions and under reasonable assumptions (which we detail in Appendix VI-A), the ZF sum-rate averaged over all time-frequency resources may be approximated as

$$\bar{\mathcal{C}}_{\mathrm{ZF}}(\mathbf{H}, \rho) \approx K \log_2 \left(1 + \frac{\rho}{K} M \bar{\xi} \right), \tag{9}$$

which links the average angle to interference factor, $\mathbf{E}\{\xi_k\} \approx \bar{\xi}$, for $k = 1, \ldots, K$, and the average channel gain,

[1] If $\sigma_1, \ldots, \sigma_K$ are the singular values of the $K \times M$ matrix $\mathbf{A}$, $K \leq M$, then $\sigma_1^2, \ldots, \sigma_K^2$ are the eigenvalues of $\mathbf{A}\mathbf{A}^{\mathrm{H}}$. Throughout the remainder of this paper, we work with both singular values and eigenvalues as we see fit.

[2] The converse is not true: favorable propagation does not imply a condition number of one. This is because users may experience different channel gains. However, in the scenarios considered in this work users are located physically close to one another and their channels tend to have similar gains.

$\mathbf{E}\{\|\mathbf{h_k}\|\}^2 \approx M$, for $k = 1, \ldots, K$, to the performance of ZF. The proof of (9) is given in Appendix VI-A. A special case of (8) is when $K = 2$. In this case, if

$$\varrho = \frac{\mathbf{h}_1^{\mathrm{H}}\mathbf{h}_2}{\|\mathbf{h}_1\| \cdot \|\mathbf{h}_2\|} \tag{10}$$

denotes the (sample) correlation coefficient of channels $\mathbf{h}_1$ and $\mathbf{h}_2$, we have the identity

$$|\varrho|^2 = 1 - \xi. \tag{11}$$

Replacing ξ with ξ_k in (11), one can view the quantity $1 - \xi_k$ as a generalization of $|\varrho|^2$ to the case of $K > 2$ users, summarizing the linear dependency between $\mathbf{h}_k$ and $\mathbf{H}_{(k)}$. We shall return to this in Sec. V.

IV. CHANNEL MEASUREMENTS AND DATA PRE-PROCESSING

This section provides an overview of the measured scenarios and the measurement setup. We also discuss the pre-processing steps applied to the measured channels.

A. MEASURED SCENARIOS

As mentioned in Sec. I, we restrict our consideration to the case where a group of users are located close to one another and concurrently communicate with a BS, mostly in LOS propagation conditions. The measurement campaigns, which we briefly describe next, took place at LTH, the Faculty of Engineering of Lund University, Lund, Sweden.

- **Open Exhibition**. Outdoor channels were measured outside the main entrance of the E-building of LTH, in a suburban environment. The BS array was mounted on a low roof, 8 m above the ground and 2 m above the roof top; see Fig. 1, left. Its lat/long coordinates are 55.711580N, 13.210285E. Nine single-antenna users confined to a 5-m diameter circle moved in random trajectories at a speed of at most 0.5 m/s; see Fig. 1, middle-top. The opening angle at the BS by the UEs is about 10° in azimuth, and 3.5° in elevation. Users were holding the antennas in front of their bodies, at about 1.3 m above the ground, with a one-handed grip. A 45° tilt was applied to as evenly as possible excite both horizontal and vertical polarizations. User sites, MS 1 and MS 2 in Fig. 1, left, have LOS to the BS, but because users were allowed to turn around, the LOS can be blocked either by the user holding the antenna or by other users. Since MS 2 offers propagation conditions fairly similar to that of MS 1, we only use measured data from MS 1 in this work. For results on MS 2, see [11], [39].
- **Crowded Auditorium**. Indoor channels were measured in room E:A of the E-building of LTH, a lecture theater with sloping floor. The BS was located at the center of the theater stage, 3.2 m above the floor. We consider four rows with five seats each; see Fig. 1, right. Nine single-antenna users were sitting on nearby seats with LOS to the BS, although the LOS was occasionally obstructed by nearby users and furniture. The opening angle at the BS by the UEs is about 14.5° in azimuth, and 10° in elevation. Users moved the antennas in irregular trajectories in front of their torsos with a one-handed grip. The trajectories covered an imaginary spherical shell about half a meter in diameter, and the revolution time was between 2 to 4 seconds; see Fig. 1, middle-bottom. As in the outdoor measurements, a downtilt of 45° was applied. In the indoor case, we expect larger angular spreads than in the outdoor environment due to more interactions with the indoor walls and ceiling. The larger angular spreads may explain the better spatial user separation reported in Sec. V.

B. MEASUREMENT SETUP

At the BS, a compact (diameter 30 cm, height 22 cm) cylindrical array with 64 dual-polarized patch antenna elements was used. The patch antenna elements are distributed in four vertically-stacked rings, with half-wavelength inter-element

FIGURE 1. (Left) Aerial photo of the outdoor measurement area showing the location of the BS (on a roof top) and the user sites (yellow circles). Users are confined to the area within the yellow circles. (Middle-top) Users at site MS 1 move in random trajectories. (Middle-bottom) Nine users sitting in lecture theater E:A. User antennas are being held with a 45° downtilt and move in random trajectories. (Right) Floor plan of lecture theater E:A.

spacing. Each patch antenna has one vertically- and one horizontally-polarized element, tallying 128 antenna ports. At the user side, 9 single-polarized omnidirectional antennas (SkyCross SMT-2TO6MB-A) were used. Note that, although user antennas are vertically-polarized and omnidirectional in azimuth when measured without user, the polarization radiation pattern when including the user's hand and body becomes more complex and is dependent on the exact user grip and orientation [40].

Fully-synchronous measurements of nine users communicating simultaneously with the 128-antenna BS array were recorded using the RUSK LUND MIMO channel sounder [41]. The transmit (Tx) unit of the RUSK LUND was connected to the user equipment (UE) antennas via dedicated radio-over-fiber links, while the BS antenna array was connected to the RUSK LUND receive (Rx) unit using a coaxial cable. The transfer functions from all users to all BS antennas were then measured at twice the Nyquist-Shannon sampling rate of the time-variant channels, to leave some room for the uncertainty in the actual velocities of the UE antennas and scatterers in the propagation environment. In the outdoor scenario, the measurement SNR varied between 10 dB (for antennas neither facing the users nor experiencing strong reflections) to 25 dB (for antennas facing the users or experiencing strong reflections), whereas in the indoor scenario, the measurement SNR varied between 18 to 25 dB. In the sequel we treat the measured channels as the true ones. Table 1 summarizes the principal parameters of the data acquisition during the measurements.

TABLE 1. Configuration parameters of RUSK LUND.

Parameter	Value
Carrier frequency	2.6 GHz
Measurement bandwidth	40 MHz
Number of subcarriers (L)	129/257[a]
Maximum measurable delay ($\tau_{\max}$)	3.2/6.4 μs[a]
Number of Tx-Rx pairs (N_{ch})	9×128
Snapshot duration	$2 \times N_{\text{ch}} \times \tau_{\max}$
Number of snapshots (N)	300
Snapshot acquisition interval	59 ms
UE output power	27 dBm

[a] Indoors/outdoors.

C. SUBARRAY AND USER SELECTION

To study the influence of the number of BS antennas on spatial user separability, subarrays with M antenna ports for $2 \leq M \leq 24$ and $M = 32, 64, 96, 128$ are formed. Imagine that the cylindrical array described above is unrolled into a matrix that has 4 rows, one for each of the stacked circles in the array, and 16 columns. Each cell in this matrix represents a dual-polarized patch antenna. If M is between 2 and 24 antenna ports, then form an M-sized subarray by selecting ports from two or more adjacent cells in the same row; subarrays should contain both horizontally- and vertically-polarized antenna ports. If $M = 32, 64, 96, 128$ ports, then one, two, three, or four adjacent rings are selected, respectively. Some examples are shown in Fig. 2.

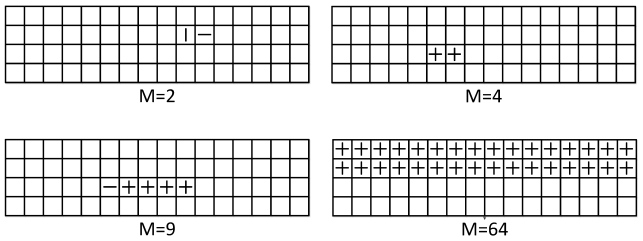

FIGURE 2. Illustration of subarray selection. The 4 × 16 matrices represent an unrolling of the cylindrical array, each cell being a dual-polarized patch antenna. Subarrays with *M* antenna ports are selected; a vertical bar ("|") identifies a selected vertically-polarized antenna port, and a dash ("–"), a selected horizontally-polarized one.

In a similar vein, groups of $K = 2, 4, 9, 18$ users are formed. If $K = 2, 4, 9$, users are drawn at random from the same measurement run. If $K = 18$, users from two measurement runs, a few minutes apart, are combined. Overall, with the above values of M and K, the systems covered in this work range from standard $K \times K$ MU-MIMO deployments at one extreme to full-blown $K \times 128$ Massive MIMO deployments at the other.

D. CHANNEL GAIN NORMALIZATION

The channel gain requirement in Sec. II can be obtained as

$$\mathbf{h}_k^{(M)}(\ell, n) = \sqrt{\frac{M \cdot N \cdot L}{\sum_{n=1}^{N} \sum_{l=1}^{L} \left\| \tilde{\mathbf{h}}_k^{(M)}(\ell, n) \right\|^2}} \tilde{\mathbf{h}}_k^{(M)}(\ell, n), \quad (12)$$

for $k = 1, \ldots, K$, where $\tilde{\mathbf{h}}_k^{(M)}(\ell, n)$ are the measured channels and the (M) superscript indicates that an M-sized subarray has been selected. With this normalization, energy variations over BS antenna elements, subcarriers and symbols are retained. In other words, the distance-dependent pathloss of the radio propagation channel is removed, whereas the effects of small-scale fading, large-scale fading, and shadowing by users are retained.

V. RESULTS AND DISCUSSION

Based on the outdoor and indoor measured channels, we present the obtained results on spatial user separability using the metrics introduced in Sec. III. To have sufficient statistics, a sample size of 1600 for each (K, M) pair of K active users and M antenna ports has been used, where samples were drawn uniformly from all available subcarriers, symbols, user combinations, and subarrays.

A. SUM-RATES

Fig. 3 compares the per-user average sum-rate of DPC, RZF and ZF, $\frac{\bar{C}_{\text{A}}(\rho)}{K}$, in bps/Hz/user, of a standard 9×9 MU-MIMO system, and 9×128 Massive MIMO, as a function of the required receive bit SNR, $\frac{E_{\text{b}}}{N_0}$. Here, subscript "A"

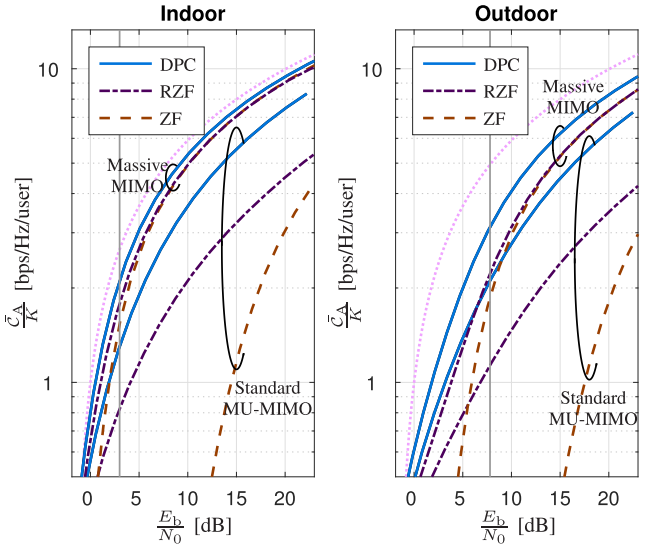

FIGURE 3. Average sum-rate vs. required bit SNR of DPC, RZF, and ZF precoding for the scaled measured channels $\frac{\mathbf{H}}{\sqrt{M}}$. There are $K = 9$ active users and $M = 9$ or 128 antennas. As a benchmark, the curve corresponding to K ideal channels (i.e., non-interfering and equally strong) is also given (dotted).

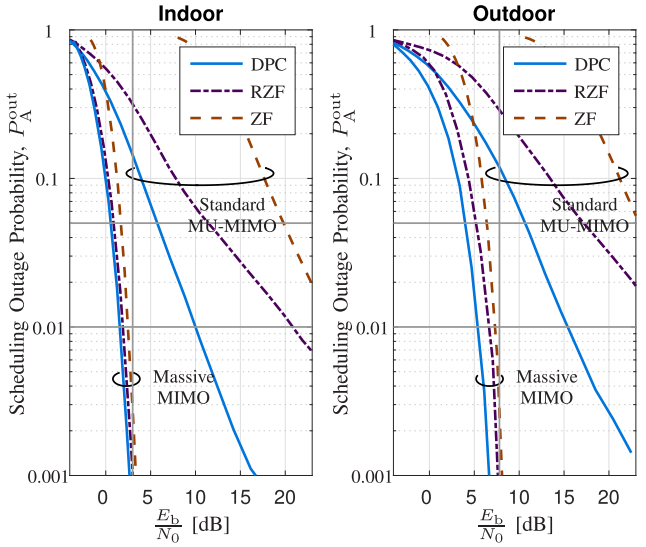

FIGURE 4. Scheduling outage probability of DPC, RZF, and ZF precoding vs. required bit SNR for the scaled measured channels $\frac{\mathbf{H}}{\sqrt{M}}$. There are $K = 9$ active users and $M = 9$ or 128 antennas.

in $\bar{C}_A(\rho)$ is one of "DPC", "RZF", or "ZF". Note that $\frac{E_b}{N_0}$ relates to the DL SNR by the formula $\rho = \frac{E_b}{N_0}\bar{C}_A(\rho)$. To facilitate the comparison, channels are scaled by dividing them by $\sqrt{M}$, so that the channel gain is removed. Sum-rate differences when going from 9 to 128 BS antennas can thus be ascribed to improved channel orthogonality. As a benchmark, we consider the sum-rate of K ideal channels (i.e., non-interfering and equally strong) with additive white Gaussian noise (AWGN).[3]

The beneficial effect of using a large number of BS antennas can be seen by considering the horizontal gap between ideal AWGN channels and realistic ones, which we call the $\frac{E_b}{N_0}$ loss. The reduction of the $\frac{E_b}{N_0}$ loss when going from standard MU-MIMO to Massive MIMO is remarkable. With RZF precoding and $M = 128$ antennas the $\frac{E_b}{N_0}$ loss is at most 2 dB (indoor channel) and 6 dB (outdoor channel) over the entire range of considered SNR values, which is admissible for many practical applications. Since in the low-SNR regime RZF approaches MRT [38], the $\frac{E_b}{N_0}$ loss decreases further as $\frac{E_b}{N_0}$ becomes smaller. In contrast, with $M = 9$ antennas the $\frac{E_b}{N_0}$ loss takes on impractically large values, except at very low values of the SNR. As expected, ZF does not perform well when $\frac{M}{K}$ is small, or at low SNR values. However, in the moderate- to high-SNR region (i.e., to the right of the vertical lines in Fig. 3) ZF performs similarly to RZF, provided that sufficiently many antennas are available at the BS. We next show that this is the region of main interest from the viewpoint of spatial user separation.

[3]This can be considered as the limiting case of DPC, RZF, and ZF as $M \to \infty$, if we allow the array to grow arbitrarily large and assume that directional properties are maintained.

In terms of achievable sum-rates, we give the following definition of spatial *multiplexing*—or *separation*—of K users. For given bit SNR $\frac{E_b}{N_0} > 0$, and $K \times M$ channel matrices $\mathbf{H}(\ell, n)$, with $\ell = 1, \ldots, L$, and $n = 1 \ldots, N$, we say that all K users can be spatially multiplexed at scheduling outage level $\eta > 0$ if the scheduling outage probability, P^{out}_{DPC}, is at most η while the total sum-rate $C_{DPC}(\mathbf{H}(\ell, n), \rho)$ is being maximized. Here, P^{out}_{DPC} is defined as the probability that a user for which there is available data is not scheduled (because that would imply a suboptimal total sum-rate). Here we assume that there is an unlimited amount of data available for each user (i.e., the full-buffer assumption holds). By definition, P^{out}_{DPC} is bounded above by $\frac{K-1}{K}$, because one can always schedule at least one user. Spatial multiplexing with RZF and ZF and the corresponding scheduling outage probabilities P^{out}_{RZF} and P^{out}_{ZF} are defined analogously.[4] Fig. 4 shows P^{out}_A as a function of the required bit SNR, whereas before "A" is one of "DPC", "RZF", or "ZF". When using standard MU-MIMO, P^{out}_A decreases slowly with increasing $\frac{E_b}{N_0}$. When using Massive MIMO, P^{out}_A drops almost vertically once a certain bit SNR value is reached. As an example, reducing P^{out}_A from 0.05 to 0.01 comes at virtually no cost with Massive MIMO, both indoors and outdoors, whereas $\frac{E_b}{N_0}$ needs to be increased by 5 to 10 dB with standard MU-MIMO, depending on the precoding scheme. There are more interesting details in the Massive MIMO regime.

[4]Other definitions are possible. One could also consider, e.g., the so-called *symmetric* rate, which is defined to be the maximum individual rate that all users can simultaneously sustain [42]–[44]. Numerical analysis of the measured channels (not shown in Fig. 3 for the sake of clarity) show that these two notions of spatial user separability are largely exchangeable: with ZF and in the bandwidth-limited region $\frac{\bar{C}_{ZF}}{K} \geq 1$ [26], the curves obtained with both definitions are fairly close to each other. Moreover, for given $\frac{\bar{C}_{ZF}}{K}$ the bit SNR gap between them tightens as M increases.

Denote by $P_{\mathrm{A}}^{\mathrm{all}}$ the probability that all K users are scheduled in the same time-frequency resource. Conditioned on the full-buffer assumption, if channels are iid, then $P_{\mathrm{A}}^{\mathrm{all}}$ relates to $P_{\mathrm{A}}^{\mathrm{out}}$ by the expression

$$P_{\mathrm{A}}^{\mathrm{all}} = (1 - P_{\mathrm{A}}^{\mathrm{out}})^K.$$

Solving $P_{\mathrm{A}}^{\mathrm{out}}$ for $P_{\mathrm{A}}^{\mathrm{all}} = 0.99$, say, yields 0.0011. In other words, if $\frac{E_{\mathrm{b}}}{N_0}$ is to the right of the vertical lines in Fig. 4, then all $K = 9$ users can be scheduled simultaneously at least 99% of the time with Massive MIMO. Again, note that the curves for RZF and ZF are close to each other in the regime of interest.

Does this mean that we need all 128 antennas, or can we get away with substantially fewer antennas? What happens if we have other numbers of users? To answer these questions we turn to Fig. 5, which gives the $\frac{E_{\mathrm{b}}}{N_0}$ losses of DPC, RZF, and ZF with respect to ideal channels (as defined above), for various numbers of BS antennas and active users. Here, we fix the average per-user rate to 2 bps/Hz, which yields instantaneous per-user rates mostly in the range from 0.5 to 4 bps/Hz, typical of wireless communication standards such as LTE [45] and IEEE 802.11 WLAN [17]. We first concentrate on the performance of RZF, in the top part of Fig. 5. Note that the $\frac{E_{\mathrm{b}}}{N_0}$ loss drops quickly as M exceeds K, and then flattens out (for small K) or decreases at a distinct, slower rate (for larger K), forming a sort of dual-slope curve. ZF precoding, in the bottom part of Fig. 5, presents a similar behavior, with larger bit SNR losses when M is close to K. The reason is that while RZF balances between maximizing received user signal power and canceling multiuser interference, ZF completely removes the latter. In doing so, ZF reduces its energy efficiency compared to RZF, especially at low SNR or when M is close to K. Naturally, one would choose M such as to at least end up beyond the "knee" of the corresponding dual-slope curve. Roughly speaking, by selecting M to be between three to four times the number of users, K, this goal is achieved; see Fig. 5. (There is some arbitrariness here in the choice of the admissible cutoff value for $\frac{E_{\mathrm{b}}}{N_0}$. Yet, the above rule of thumb provides a useful estimate of the size of M that reaps most of the available gain). Lastly, we note that the $\frac{E_{\mathrm{b}}}{N_0}$ loss increases with K, for all of DPC, RZF, and ZF: The price to pay for serving more users is that one must send energy in less "good" directions, so much so that increasingly less effective channels need to be used the more users one desires to separate.

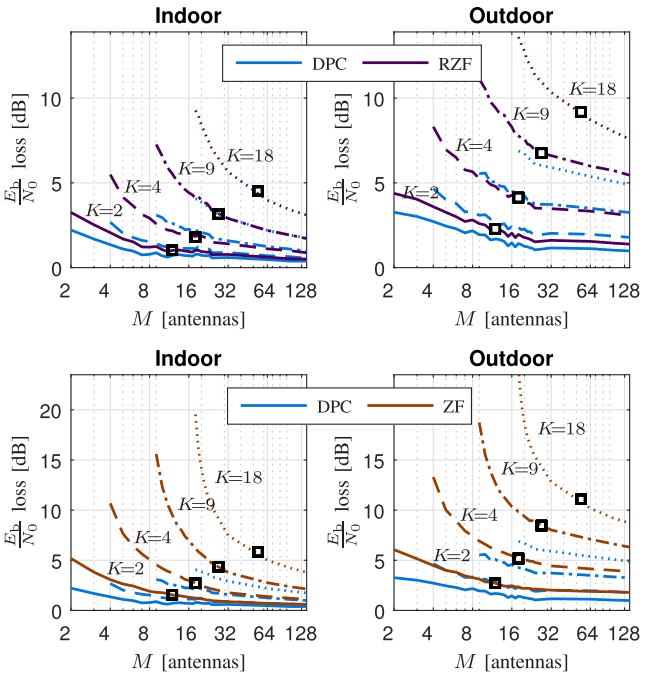

FIGURE 5. Bit SNR loss of DPC, RZF (top), and ZF (bottom) for the scaled measured channels $\frac{\mathbf{H}}{\sqrt{M}}$. Here, we fix $\frac{C_{\mathrm{A}}}{K} = 2$ bps/Hz/user, and vary the number of BS antennas, M, and active users, K. Square markers indicate the suggested size of M.

B. CHANNEL CONDITION NUMBER AND SMALLEST SINGULAR VALUE

Fig. 6 shows the 10th, 50th, and 90th percentiles of the logarithm, κ_{dB}, of the channel condition number. Values of κ_{dB} are plotted as a function of the ratio $\beta = \frac{K}{M}$ for $K = 2, 4, 9, 18$ active users. We observe that for given K, its median, $\kappa_{\mathrm{dB}}^{(50)}$, decreases steadily as M grows larger (or equivalently, as β decreases). It demonstrates that with practical channels, adding BS antennas helps decreasing the channel condition number, thereby improving spatial user separability. The rate of decrease is largest at $\beta = 1$. In general, for given β, $\kappa_{\mathrm{dB}}^{(50)}$ is smaller for indoor than for outdoor channels. This is expected since, as pointed out earlier, indoor channels typically enjoy richer scattering due to more interactions with

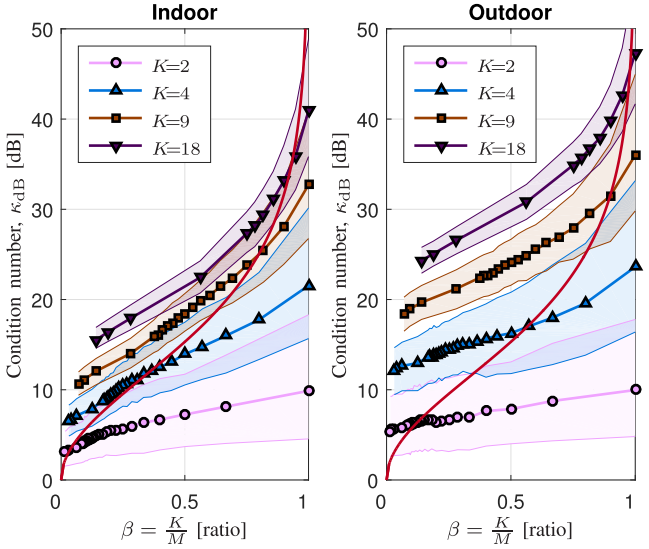

FIGURE 6. The 10th, 50th, and 90th percentiles of κ_{dB} as a function of $\beta = \frac{K}{M}$ for various numbers of users, K. Users are located close to one another in LOS propagation conditions in an indoor environment (left), and in an outdoor environment (right). For comparison, the condition number (13) for iid Rayleigh channels has also been plotted (red solid line).

walls and furniture [46]. Not only does the median of κ_{dB} decrease with M, but also its spread, defined here as the difference $\kappa_{\text{dB}}^{(90)} - \kappa_{\text{dB}}^{(10)}$ between the 90$^{\text{th}}$ and 10$^{\text{th}}$ percentiles. For all K, the spread of κ_{dB} is roughly 14 dB (indoor) and 16 dB (outdoor) at $\beta = 1$, and then decreases to just a few units of decibels as M grows larger. In other words, as M increases κ_{dB} tends to concentrate around its mean. This effect, an instance of a large-systems phenomenon known as *channel hardening* [25], [47], leads to important simplifications of certain system aspects including user resource allocation, power control, and interference management [2], [5], [48], and is thus desirable.

It is interesting to compare results obtained from measured channels with those from a random matrix with iid entries $\mathcal{CN}(0, 1)$, i.e., iid Rayleigh channels, often assumed in theoretical studies. For the latter, we use the following asymptotic result [49, Th. 6.3] for the logarithm of the condition number:

$$\mathbf{E}\left\{\kappa_{\text{dB,iid}}\right\} = 20\log_{10}\left(\frac{1+\sqrt{\beta}}{1-\sqrt{\beta}}\right) + o(1) \tag{13}$$

whenever $M, K \to \infty$ such that $\frac{K}{M} \to \beta \in (0, 1)$.[5] The limit (13) has been plotted in Fig. 6 (in red). The discrepancy between results obtained from iid Rayleigh and measured channels is apparent, the former being too poor a predictor of the latter, even as K increases. In general, better agreement can be observed in the case of indoor propagation with rich scattering (see, e.g., $K = 9, 18$), but a substantial gap between measured and iid Rayleigh channels remains for small β. Basically, since we are working with LOS measurements, κ_{dB} does not come close to what is expected from iid Rayleigh channels in the Massive MIMO region. We also make a note that while (13) depends only on the ratio $\beta = \frac{K}{M}$, this ratio alone is not sufficient to characterize κ_{dB} computed from the measured channels, as the latter depends strongly on K.

Next, we study the operational significance of the channel condition number and the smallest singular value to Massive MIMO systems. For simplicity, let us restrict our attention to the uplink of a system with K single-antenna users. The following result shows that SNR averaged over all users at the output of a ZF receiver, $\rho_{\text{ul}}^{\text{ZF}}$, can be expressed in terms of only the transmit SNR, ρ_{ul}, and the eigenvalues $\sigma_1^2 \geq \ldots \geq \sigma_K^2$ of $\mathbf{H}\mathbf{H}^{\text{H}}$. In particular, we have

$$\rho_{\text{ul}}^{\text{ZF}} = \left(\frac{\sum_{k=1}^{K} 1/\sigma_k^2}{K}\right)^{-1} \cdot \rho_{\text{ul}}. \tag{14}$$

A derivation of (14) can be found in Appendix VI-B. For the studied scenarios of closely located users in LOS, in which users experience similar propagation conditions in the measurement environment, we expect the post-processing SNR of the individual users to be close to $\rho_{\text{ul}}^{\text{ZF}}$. Basically, (14) asserts that the power transfer function from each user to the output of the ZF receiver, denoted $\gamma = \frac{\rho_{\text{ul}}^{\text{ZF}}}{\rho_{\text{ul}}}$, is simply the harmonic mean $H(\sigma_1^2, \ldots, \sigma_K^2)$ of the eigenvalues. It follows from the properties of the harmonic mean that

$$\sigma_K^2 \leq \gamma \leq K \cdot \sigma_K^2. \tag{15}$$

and so the smallest eigenvalue, σ_K^2, dominates uplink performance whenever it is close to zero. Note that it is possible for γ to be greater than one if there is array gain. Using that the harmonic mean $H(x_1, \ldots, x_n)$ of n non-negative numbers $x_1, \ldots, x_n$ is never greater than the arithmetic mean $A(x_1, \ldots, x_n)$, and that $\frac{1}{K}\sum_{k=1}^{K}\sigma_k^2 \leq \sigma_1^2$, we can sharpen (15) to

$$\sigma_K^2 \leq \gamma \leq \min(\kappa^2, K) \cdot \sigma_K^2, \tag{16}$$

which relates uplink performance to both the channel condition number, κ, and the smallest singular value, σ_K.

We can further explore, empirically, the relation between uplink performance and channel condition number. This is illustrated in Fig. 7, which shows the median of the logarithm of γ, denoted $\gamma_{\text{dB}}^{(50)}$, as a function of $\kappa_{\text{dB}}^{(50)}$ for various choices of K and M. Note that, as in Fig. 3 to Fig. 5, channels have been scaled by dividing them by $\sqrt{M}$. Clearly, there is a strong correlation between these two quantities, and $\kappa_{\text{dB}}^{(50)}$ could be used to predict $\gamma_{\text{dB}}^{(50)}$ to some extent, if so desired. Lower values of $\kappa_{\text{dB}}^{(50)}$ translate directly into larger values of $\gamma_{\text{dB}}^{(50)}$, and thus improved spatial separability of the users. Note that for given $\kappa_{\text{dB}}^{(50)}$, the corresponding $\gamma_{\text{dB}}^{(50)}$ is smaller with indoor propagation than with iid Rayleigh channels, and it is smallest in outdoor propagation. The reason is that the eigenvalues $\sigma_1^2 \geq \ldots \geq \sigma_K^2$ are spaced more evenly in the iid Rayleigh case than they are in the measured channels. This unequal spacing of the eigenvalues is mainly due to the presence of strong LOS components in the measured

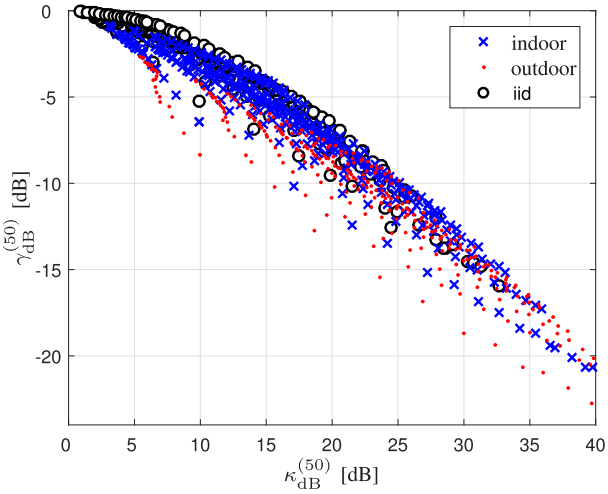

FIGURE 7. Median of the logarithm of the ZF uplink power transfer function, $\gamma_{\text{dB}}^{(50)}$, versus median of the logarithm of the channel condition number, $\kappa_{\text{dB}}^{(50)}$, of $\frac{\mathbf{H}}{\sqrt{M}}$. Each point corresponds to a pair (K, M) of K users and M BS antennas.

[5] Let functions f, g depend on a parameter n. We write $f = o(g)$ if $|f| \leq c(n)g$ for some c that goes to zero as $n \to \infty$.

channels, which induce some dominant eigenmodes, thereby skewing γ toward σ_K^2 (see (16)).

We can also say something about the degradation of γ when the number of active users is increased from $K-1$ to K. For that, we write $\mathbf{H} = \left[\mathbf{H}_{(K-1)}^{\mathrm{T}} \ \mathbf{h}_K\right]^{\mathrm{T}}$, where the matrix $\mathbf{H}_{(K-1)}$ contains the first $K-1$ rows of $\mathbf{H}$, and note that

$$\mathbf{H}\mathbf{H}^{\mathrm{H}} = \begin{bmatrix} \mathbf{H}_{(K-1)}\mathbf{H}_{(K-1)}^{\mathrm{H}} & \mathbf{H}_{(K-1)}\mathbf{h}_K^{*} \\ \mathbf{h}_K^{\mathrm{T}}\mathbf{H}_{(K-1)}^{\mathrm{H}} & \mathbf{h}_K^{\mathrm{T}}\mathbf{h}_K^{*} \end{bmatrix}. \tag{17}$$

Then, by applying the Cauchy interlacing law [50], which asserts that $\sigma_{k+1}^2(\mathbf{H}\mathbf{H}^{\mathrm{H}}) \leq \sigma_k^2(\mathbf{H}_{(K-1)}\mathbf{H}_{(K-1)}^{\mathrm{H}}) \leq \sigma_k^2(\mathbf{H}\mathbf{H}^{\mathrm{H}})$ for all $1 \leq k \leq K$, and doing some algebraic manipulations, the following result can be obtained:

$$\left(\frac{1}{\sigma_K^2(\mathbf{H}\mathbf{H}^{\mathrm{H}})} + \frac{K-1}{\gamma_{K-1}}\right)^{-1} \leq \frac{\gamma_K}{K} \leq \left(\frac{1}{\sigma_1^2(\mathbf{H}\mathbf{H}^{\mathrm{H}})} + \frac{K-1}{\gamma_{K-1}}\right)^{-1}, \tag{18}$$

where γ_{K-1} and γ_K are the uplink power transfer functions of systems with $K-1$ and K active users, respectively. Equation (18) shows that γ_K is bounded by the harmonic mean of γ_{K-1} and the extreme eigenvalues of $\mathbf{H}\mathbf{H}^{\mathrm{H}}$ (subject to proper weighting). In particular, users can be added to the system at negligible cost as long as the smallest eigenvalue, σ_K^2, is well bounded away from zero.

Fig. 8 shows that increasing the number of BS antennas, M, does indeed provide an effective way of achieving $\sigma_K^2 \gg 0$ with high probability. In this figure, empirical probability density functions (PDFs) of the eigenvalues $\sigma_1^2 \geq \ldots \geq \sigma_K^2$ of $\frac{1}{M}\mathbf{H}\mathbf{H}^{\mathrm{H}}$ are shown for $K = 9$ users, and $M = 9, 16, 128$ BS antennas. We find that as M increases, not only does the difference between the largest and the smallest eigenvalues shrink, but the PDFs of the individual eigenvalues concentrate around their means. This concentration of probability mass around the means and away from the tails is most evident for the smallest eigenvalue, σ_K^2. Roughly, its spread (measured as before as the difference between the 90$^{\text{th}}$ and the 10$^{\text{th}}$ percentiles) reduces from 14 to 4.5 to 2 dB when M increases from 9 to 16 to 128 BS antennas; see Table 2. Most important, as M increases, the PDF of σ_K^2 is effectively bounded away from zero. The concentration of probability mass phenomenon is less pronounced, however, for the larger eigenvalues. This is especially so in the outdoor propagation scenario, in which case a distinct gap is present between the two strongest eigenvalues and the bulk of the channel spectrum, irrespective of M. This behavior can also be observed in the indoor case, although to a lesser extent. This suggests that the behavior of the strong eigenvalues is primarily determined by LOS and specular components, while eigenvalues at the other edge of the spectrum are mostly influenced by diffuse propagation mechanisms.[6]

[6]We have confirmed this point empirically by extracting the direction of incidence (at the BS) associated with the eigenvectors of the measured channels. It was observed that strong eigenvectors would consistently propagate in the direction of LOS, as well as that of the strongest scattering surfaces, in the indoor case. On the other hand, weak eigenvalues would fluctuate among directions of various (weaker) scatterers.

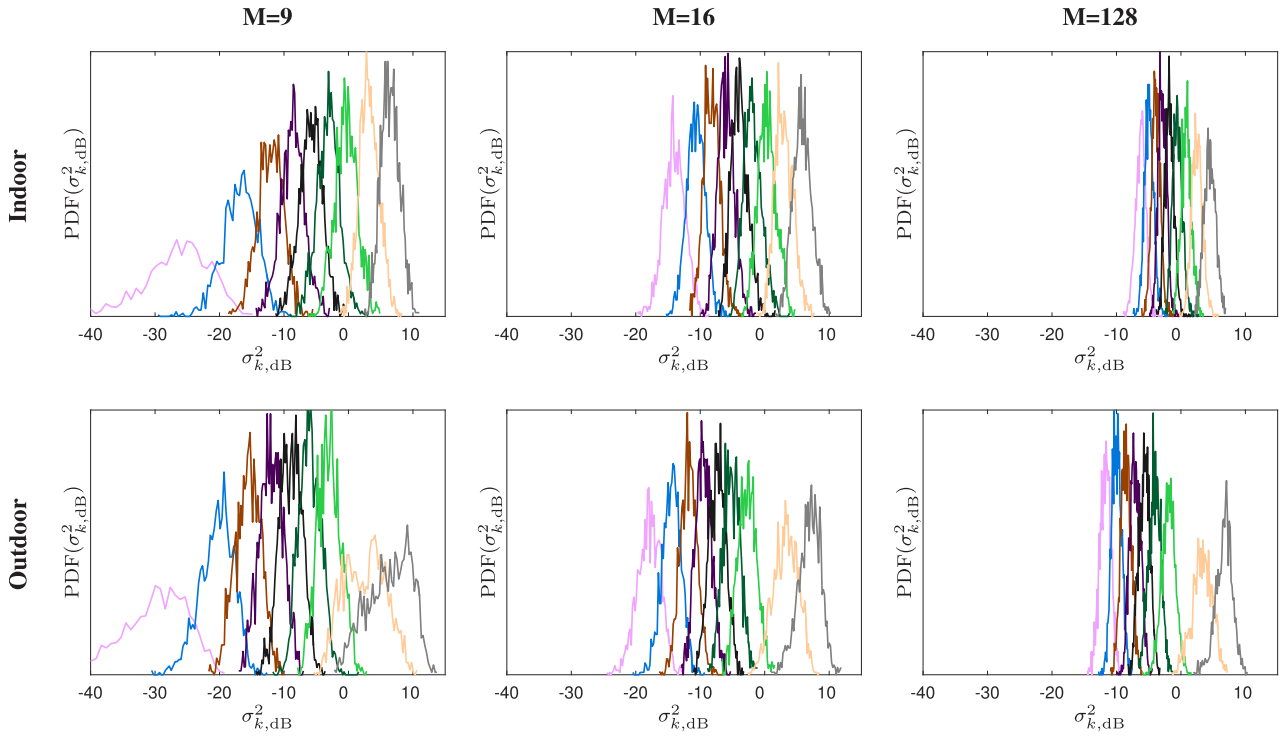

FIGURE 8. The empirical PDFs of the ordered eigenvalues of $\frac{1}{M}\mathbf{H}\mathbf{H}^{\mathrm{H}}$ for $K = 9$ active users and some selected numbers of BS antennas, M. Here, $\sigma^2_{k,\mathrm{dB}}$ has been computed as $10\log_{10}\sigma_k^2$, with σ_k^2 the k^{th} largest eigenvalue.

TABLE 2. Difference between 90th and 10th percentiles of $\sigma^2_{k,\mathrm{dB}}$.

Scenario	Number of BS antennas		
	$M = 9$	$M = 16$	$M = 128$
Indoor			
$k = 1$	3.79	3.77	2.31
$k = 9$	14.00	4.32	2.08
Outdoor			
$k = 1$	8.84	4.42	3.20
$k = 9$	14.10	4.61	2.20
iid Gaussian			
$k = 1$	1.60	1.34	0.56
$k = 9$	12.98	3.52	0.75

C. ANGLE TO INTERFERENCE SUBSPACE

We now discuss spatial user separability in terms of the angle to interference factor, ξ, defined by (8). Recall that we would like to have ξ close to one. Fig. 9 shows the 10th, 50th, and 90th percentiles of ξ as a function of $\beta = \frac{K}{M}$. For a fixed number K of active users, increasing the number of BS antennas, M, increases the median of ξ, hereafter denoted $\xi^{(50)}$, and thus improves spatial user separability. This increase is particularly substantial when K is large or moderately large. Consider the case of $K = 9$ active users outdoors, for instance. By increasing M from 9 to 16, it is possible to raise $\xi^{(50)}$ from about 0.03 to 0.14, which represents a five-fold improvement with respect to a standard 9×9 MU-MIMO system; even better, setting M equal 128 yields a whopping 12-fold improvement. Thus, with respect to ξ, the larger K, the more beneficial an excess of BS antennas $M > K$ becomes.

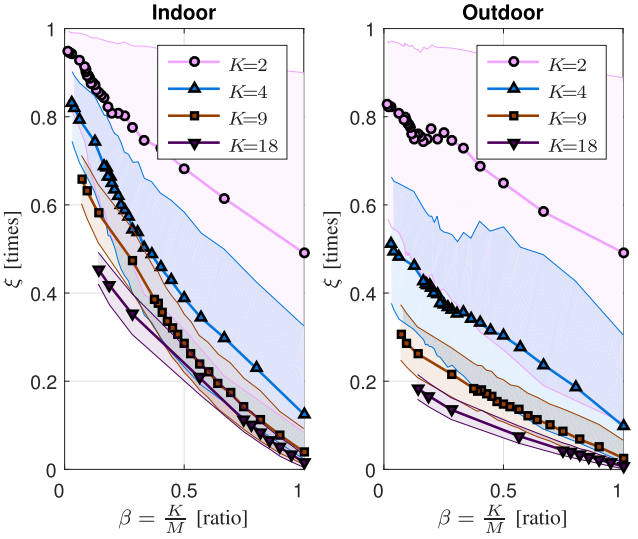

FIGURE 9. The 10th, 50th, and 90th percentiles of the angle to interference factor, ξ, for various numbers of active users, K, and BS antennas, M. The users are located close to one another in LOS propagation conditions in an indoor environment (left), and in an outdoor environment (right).

For given β, we find that $\xi^{(50)}$ is larger for indoor propagation than for outdoor, which is likely due to typically larger angular spreads in indoor environments, as mentioned in Sec. V-B. We also note that the spread of ξ decreases as either the number of BS antennas, M, or the number of active users, K, increase (although $\xi^{(50)}$ itself does of course decrease—it gets worse—as K increases). This suggests that adding users to the system is actually beneficial to stabilize performance, at least in the case of closely located users with LOS, as we observe here. In fact, K appears to have a larger impact than M on the spread of ξ. The reason is that for a given ratio β, adding users increases the number of independent channel realizations, thereby resulting in a notable reduction of the spread of ξ, as evidenced by Fig. 9. In the studied scenarios, adding BS antennas is less effective at reducing the spread of ξ because they tend to be correlated.

As a practical note, we present a possible application of the data reported in Fig. 9. Essentially, we propose a mapping between pairwise correlation coefficients, $|\varrho|$, defined in Sec. III-C, and angles to interference subspace, ξ. Because of its relatively low computational complexity, the correlation coefficient $|\varrho|$ of two users is sometimes favored in practical multiuser scheduling algorithms [51]–[53]. For example, it is proposed in [53] that K users be scheduled in the same time-frequency resource if $|\varrho_{ij}|^2 \leq |\varrho_{\mathrm{th}}|^2 (1 \leq i < j \leq K)$ is upheld, where $0 \leq |\varrho_{\mathrm{th}}| \leq 1$ is a threshold parameter that trades off signal-to-interference ratio and communication latency. The value $|\varrho_{\mathrm{th}}| = 0.3$ is suggested for certain array geometries [53]. In general, finding a suitable value of $|\varrho_{\mathrm{th}}|$ is not straightforward. Alternatively, the scheduling algorithm might place a constraint on ξ. For instance, by virtue of (11), the equivalent condition $\xi_{\mathrm{th}} \geq 1 - |\varrho_{\mathrm{th}}|^2$ is obtained for $K = 2$. In fact, this approach has the advantage that ξ can be directly related to system performance through (9), from which an appropriate threshold ξ_{th} can be readily obtained for arbitrary K. Directly evaluating ξ is, however, comparatively more difficult for $K > 2$, as one must invert $\mathbf{H}\mathbf{H}^{\mathrm{H}}$ for the various sets of users considered for concurrent communication. Nonetheless, much of this complexity can be offloaded. All that is required is a lookup mechanism that maps the required threshold ξ_{th} to some $|\varrho_{\mathrm{th}}|$, which can then be used with, e.g., the scheduling algorithm proposed in [53]. Such a lookup-table can be easily extracted from Fig. 9. The following example illustrates how this can be accomplished.

Example: Let $K = 4$, $\xi^{(50)}_{\mathrm{th}} = \frac{1}{3}$, and assume indoor propagation. From Fig. 9, we have $\beta \leq \frac{2}{3}$, which requires $M \geq 6$. We then read off from the curve $K = 2$ the abscissa value at $\beta' = \frac{2}{M} = \frac{1}{3}$, which is 0.75. Last, we compute the desired threshold as $|\varrho_{\mathrm{th}}|^2 = 1 - 0.75 = 0.25$. If $K = 9$ instead, we can proceed in an analogous manner, in which case we obtain $|\varrho_{\mathrm{th}}|^2 = 0.11$ (now one needs $M \geq 19$). This example illustrates that for fixed $\xi^{(50)}_{\mathrm{th}}$, the associated threshold, $|\varrho_{\mathrm{th}}|^2$, and required number of BS antennas, M, can vary significantly depending on the target number of concurrently served users, K.

Fig. 9 can also be interpreted as follows: For given K, there is an orthogonality gain $\frac{\xi(\beta)}{\xi(1)}$ of a system with $M > K$ over one with $M = K$ BS antennas; in general, the orthogonality

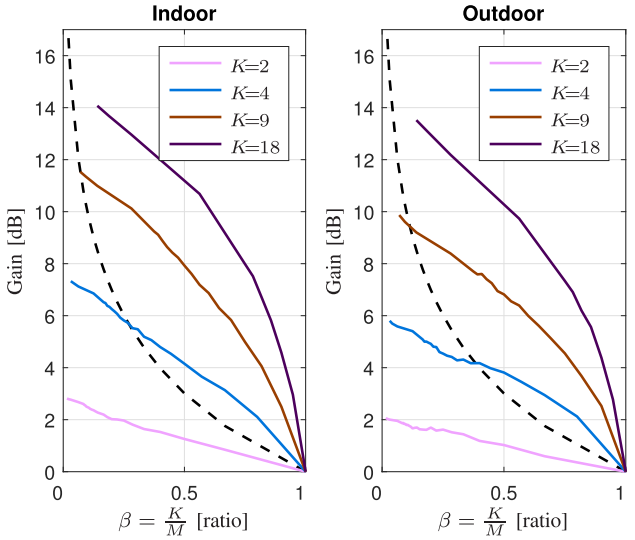

FIGURE 10. The orthogonality gain (solid line) and the array gain (dashed line) of a $K \times M$ system relative to a standard $K \times K$ MU-MIMO system, as estimated from indoor and outdoor measured channels.

gain increases whenever the number of BS antennas, M, is increased. How does the orthogonality gain compare to the array gain, which is roughly $\frac{M}{K}$ for the same numbers of antennas? The two gains are compared in Fig. 10. The important thing to note is that the orthogonality gain and the array gain complement each other. Let us ignore for a moment the case of $K = 2$ users. When β is close to one, orthogonality gains dominate, and therefore increasing M helps mostly by increasing the separation between the users' subspaces. As β approaches zero, array gain improvements eventually prevail, and further adding antennas to the system brings about a mere power saving. In this sense, there is much to be gained from spending, at least, M^* antennas, M^* being at the intercept point of the two gains for given K. By operating with M^* antennas most of the orthogonality gain can be harvested; and beyond this point more is still to be gained in terms of array gain boost. For example, when $K = 4$ active users, we have $M^* = 12$ antennas for both indoor and outdoor propagation; when $K = 9$ users, the orthogonality gain and the array gain only even up at about $M^* = 128$ antennas. Let us now return to the case of $K = 2$ active users. Here the orthogonality gain improves less than the array gain, for all $0 \leq \beta \leq 1$. This is because the measured 2×2 systems can already spatially separate two users reasonably well, on average. Nevertheless, adding antennas can significantly reduce the *spread* of the users' correlation coefficient, as demonstrated by Fig. 9.

VI. CONCLUSIONS

Using fully-synchronous measured channels at 2.6 GHz, we have investigated the ability of Massive MIMO systems to spatially separate nine or eighteen users located close to one another in LOS propagation conditions, in both indoor and outdoor environments. In particular, we evaluated the condition number of the channel matrix, the achievable sum-rates of DPC, RZF, and ZF, and the angle to interference factor as metrics of spatial user separability. Each metric covers different aspects of spatial user separability and together they provide a more comprehensive picture. The scenarios considered have been recognized as important yet challenging for future communication systems. Contrary to what can be expected from the geometry of the problem, our results show that Massive MIMO with RZF or ZF can spatially separate nine, even eighteen, concurrent users in the particularly difficult case of dominant LOS propagation. With indoor propagation and at 2 bps/Hz per user, SNR losses relative to ideal channels can be made as small as 2 and 4 dB for nine and eighteen concurrent users, respectively (cf. 16 and 20 dB for fully-loaded traditional MU-MIMO systems). Furthermore, we quantified the amount of antennas that are required to spatially separate concurrent users. Our findings suggest that with RZF or ZF a factor three to four between the number of BS antennas and the number of concurrently served users is sufficient. For these numbers of antennas and users, the main contribution to improving system performance, measured in sum-rates, comes from the orthogonality gain afforded by Massive MIMO, although in general the orthogonality gain and the array gain complement each other. Finally, we have used the angle to interference factor as a metric of spatial user separability which can be directly linked to the performance of ZF; novel expressions relating the smallest singular value of a multiuser MIMO channel with the performance of ZF have also been provided.

APPENDIX

A. PROOF OF (9)

We start by writing the average ZF sum-rate as

$$\bar{\mathcal{C}}_{\mathrm{ZF}}(\rho) = \frac{1}{T}\sum_{i=1}^{T}\sum_{k=1}^{K}\log_2\left(1+\rho\lambda_{i,k}g_{i,k}^2\right),$$

where the index i runs over T time-frequency resources, $\lambda_{i,k} = (1/\mu_i - 1/g_{i,k}^2)^+$ are waterfilling coefficients with $\lambda_{i,k} \geq 0$ and $\lambda_{i,1} + \cdots + \lambda_{i,K} = 1$, for some $\mu_i \geq 0$ and $i = 1, \ldots, T$, and whereas $(x)^+ = \max(x, 0)$. Since $\log(1 + x)$ is concave for $x \geq 1$, we see from Jensen's inequality[7] that

$$\bar{\mathcal{C}}_{\mathrm{ZF}}(\mathbf{H}, \rho) \leq K \cdot \log_2\left(1 + \frac{1}{T}\frac{1}{K}\sum_{i=1}^{T}\sum_{k=1}^{K}\rho\lambda_{i,k}g_{i,k}^2\right).$$

It is well-known that for sufficiently high SNR, ρ, one has $\lambda_{i,k} \approx 1/K$. Now, if we make the assumption that user channels are statistically identical in the indices i and k (which is reasonable for the studied scenarios of closely-located users moving randomly within a limited area), and thus $g_{i,k}^2 \sim g^2$, we have $\frac{1}{T}\frac{1}{K}\sum_{i=1}^{T}\sum_{k=1}^{K}(\rho\lambda_{i,k}g_{i,k}^2) \to \frac{\rho}{K}\mathbf{E}\{g^2\}$ as $T \to \infty$

[7] Jensen's inequality asserts that [54] if f is concave, $x_1, \ldots, x_n$ are in the domain of f, and $\theta_1, \ldots, \theta_n \geq 0$ with $\theta_1 + \cdots + \theta_n = 1$, then

$$f(\theta_1 x_1 + \cdots + \theta_n x_n) \geq \theta_1 f(x_1) + \cdots + \theta_n f(x_n).$$

by the law of large numbers. In general, we may assume that channel gains $\|\mathbf{h}\|^2$ and angles θ are uncorrelated, and thus $\mathbf{E}\{g^2\} = \mathbf{E}\{\|\mathbf{h}\|^2\}\mathbf{E}\{\xi\}$. The desired result (9) follows by using $\|\mathbf{h}\|^2 \to M$ as $T \to \infty$, as demanded in Sec. II.

B. DERIVATION OF (14)

Consider the uplink model

$$\mathbf{y} = \sqrt{E_\mathrm{s}}\mathbf{G}\mathbf{x} + \mathbf{n}, \tag{19}$$

where $\mathbf{x} \in \mathbb{C}^{K\times 1}$ contains the transmitted data symbols $x_1, \ldots, x_K$ satisfying $\overline{|x_k|^2} = \lim_{T\to\infty} \frac{1}{T}\sum_{i=1}^{T} |x_k|^2 = 1$, i.e., users transmit with unit average energy per time-frequency resource, $\mathbf{G} \in \mathbb{C}^{M\times K}$ is the uplink channel matrix, assumed to be known at the BS, $\mathbf{n} \in \mathbb{C}^{M\times 1}$ the vector of receiver noise with iid $\mathcal{CN}(0, N_0)$ entries, and $\mathbf{y} \in \mathbb{C}^{M\times 1}$ the vector of received samples for baseband processing. Define the transmit SNR by $\rho_\mathrm{ul} = \frac{E_\mathrm{s}}{N_0}$. The signal at the output of the ZF receiver can be written as

$$\hat{\mathbf{x}}_\mathrm{ZF} = \sqrt{\alpha}(\mathbf{G}^\mathrm{H}\mathbf{G})^{-1}\mathbf{G}^\mathrm{H}\mathbf{y} \tag{20}$$

$$= \sqrt{\alpha E_\mathrm{s}}\mathbf{x} + \sqrt{\alpha}(\mathbf{G}^\mathrm{H}\mathbf{G})^{-1}\mathbf{G}^\mathrm{H}\mathbf{n}. \tag{21}$$

The noise covariance matrix of $\hat{\mathbf{x}}_\mathrm{ZF}$ is

$$\mathrm{Cov}\left(\hat{\mathbf{x}}_\mathrm{ZF}\right) = \alpha\left(\mathbf{G}^\mathrm{H}\mathbf{G}\right)^{-1} N_0, \tag{22}$$

Thus, if we let $\alpha = K \cdot \mathrm{tr}\left((\mathbf{G}^\mathrm{H}\mathbf{G})^{-1}\right)^{-1}$, we have

$$\frac{1}{K}\sum_{k=1}^{K} \mathrm{Var}\left(\hat{x}_{\mathrm{ZF},k}\right) = \frac{1}{K}\mathrm{tr}\left(\mathrm{Cov}\left(\hat{\mathbf{x}}_\mathrm{ZF}\right)\right) = N_0. \tag{23}$$

Similarly, we obtain

$$\frac{1}{K}\sum_{k=1}^{K} \alpha E_\mathrm{s}\overline{|x_k|^2} = \left(\frac{\sum_{k=1}^{K} 1/\sigma_k^2}{K}\right)E_\mathrm{s}. \tag{24}$$

From equations (23) and (24), the SNR at the output of the ZF receiver averaged over all the users may be computed as

$$\rho_\mathrm{ul}^\mathrm{ZF} = \frac{\frac{1}{K}\sum_{k=1}^{K} \alpha E_\mathrm{s}\overline{|x_k|^2}}{\frac{1}{K}\sum_{k=1}^{K} \mathrm{Var}\left(\hat{x}_{\mathrm{ZF},k}\right)} \tag{25}$$

$$= \left(\frac{\sum_{k=1}^{K} 1/\sigma_k^2}{K}\right)^{-1} \rho_\mathrm{ul}, \tag{26}$$

which is precisely (14).

ACKNOWLEDGMENT

The authors would like to thank all the participants in the measurement campaigns for their contributions to the measurements.

REFERENCES

[1] T. L. Marzetta, "Noncooperative cellular wireless with unlimited numbers of base station antennas," *IEEE Trans. Wireless Commun.*, vol. 9, no. 11, pp. 3590–3600, Nov. 2010.
[2] F. Rusek *et al.*, "Scaling up MIMO: Opportunities and challenges with very large arrays," *IEEE Signal Process. Mag.*, vol. 30, no. 1, pp. 40–60, Jan. 2013.
[3] E. G. Larsson, O. Edfors, F. Tufvesson, and T. L. Marzetta, "Massive MIMO for next generation wireless systems," *IEEE Commun. Mag.*, vol. 52, no. 2, pp. 186–195, Feb. 2014.
[4] H. Q. Ngo, E. G. Larsson, and T. L. Marzetta, "Energy and spectral efficiency of very large multiuser MIMO systems," *IEEE Trans. Commun.*, vol. 61, no. 4, pp. 1436–1449, Apr. 2013.
[5] T. L. Marzetta, E. G. Larsson, H. Yang, and H. Q. Ngo, *Fundamentals of Massive MIMO*. Cambridge, U.K.: Cambridge Univ. Press, 2016.
[6] J. G. Andrews *et al.*, "What will 5G be?" *IEEE J. Sel. Areas Commun.*, vol. 32, no. 6, pp. 1065–1082, Jun. 2014.
[7] F. Boccardi, R. W. Heath, Jr., A. Lozano, T. L. Marzetta, and P. Popovski, "Five disruptive technology directions for 5G," *IEEE Commun. Mag.*, vol. 52, no. 2, pp. 74–80, Feb. 2014.
[8] M. Shafi *et al.*, "5G: A tutorial overview of standards, trials, challenges, deployment, and practice," *IEEE J. Sel. Areas Commun.*, vol. 35, no. 6, pp. 1201–1221, Jun. 2017.
[9] T. L. Marzetta, "How much training is required for multiuser MIMO," in *Proc. 40th Asilomar Conf. Signals, Syst. Comput. (ACSSC)*, Pacific Grove, CA, USA, Nov./Dec. 2006, pp. 359–363.
[10] X. Gao, O. Edfors, F. Rusek, and F. Tufvesson, "Massive MIMO performance evaluation based on measured propagation data," *IEEE Trans. Wireless Commun.*, vol. 14, no. 7, pp. 3899–3911, Jul. 2015.
[11] J. Flordelis, X. Gao, G. Dahman, F. Rusek, O. Edfors, and F. Tufvesson, "Spatial separation of closely-spaced users in measured massive multi-user MIMO channels," in *Proc. IEEE Int. Conf. Commun. (ICC)*, London, U.K., Jun. 2015, pp. 1441–1446.
[12] P. Harris *et al.*, "Performance characterization of a real-time massive MIMO system with LOS mobile channels," *IEEE J. Sel. Areas Commun.*, vol. 35, no. 6, pp. 1244–1253, Jun. 2017.
[13] S. Malkowsky *et al.*, "The world's first real-time testbed for massive MIMO: Design, implementation, and validation," *IEEE Access*, vol. 5, pp. 9073–9088, 2017.
[14] A. Osseiran *et al.*, "Scenarios for 5G mobile and wireless communications: The vision of the METIS project," *IEEE Commun. Mag.*, vol. 52, no. 5, pp. 26–35, May 2014.
[15] E. Karipidis, J. Lorca, and E. Björnson, "D1.1: System scenarios and requirements specifications," Mammoet, Utrecht, The Netherlands, Tech. Rep. ICT-619086-D1.1, 2015.
[16] *LTE Standardization Body*, 3GPP.
[17] *IEEE Standard for Information Technology—Telecommunications and Information Exchange Between Systems Local and Metropolitan Area Networks—Specific requirements—Part 11: Wireless LAN Medium Access Control (MAC) and Physical Layer (PHY) Specifications*, IEEE Standard 802.11, 2016.
[18] X. Gao, F. Tufvesson, and O. Edfors, "Massive MIMO channels—Measurements and models," in *Proc. IEEE Asilomar Conf. Signals, Syst. Comput.*, Nov. 2013, pp. 280–284.
[19] X. Gao, O. Edfors, F. Tufvesson, and E. G. Larsson, "Massive MIMO in real propagation environments: Do all antennas contribute equally?" *IEEE Trans. Commun.*, vol. 63, no. 11, pp. 3917–3928, Nov. 2015.
[20] S. Payami and F. Tufvesson, "Channel measurements and analysis for very large array systems at 2.6 GHz," in *Proc. 6th Eur. Conf. Antennas Propag. (EUCAP)*, Prague, Czech Republic, Mar. 2012, pp. 433–437.
[21] X. Gao, O. Edfors, F. Rusek, and F. Tufvesson, "Linear pre-coding performance in measured very-large MIMO channels," in *Proc. IEEE Veh. Technol. Conf. (VTC)*, Sep. 2011, pp. 1–5.
[22] J. Hoydis, C. Hoek, T. Wild, and S. ten Brink, "Channel measurements for large antenna arrays," in *Proc. IEEE 9th Int. Symp. Wireless Commun. Syst. (ISWCS)*, Aug. 2012, pp. 811–815.
[23] M. Gauger, J. Hoydis, C. Hoek, H. Schlesinger, A. Pascht, and S. ten Brink, "Channel measurements with different antenna array geometries for massive MIMO systems," in *Proc. 10th Int. ITG Conf. Syst., Commun. Coding (SCC)*, Feb. 2015, pp. 1–6.
[24] A. O. Matínez, E. De Carvalho, and J. Ø. Nielsen, "Towards very large aperture massive MIMO: A measurement based study," in *Proc. Global Telecommun. Conf. (GLOBECOM)*, Dec. 2014, pp. 281–286.
[25] A. O. Matínez, E. De Carvalho, and J. Ø. Nielsen, "Massive MIMO properties based on measured channels: Channel hardening, user decorrelation and channel sparsity," in *Proc. Asilomar 50th Conf. Signals, Syst. Comput.*, Nov. 2016, pp. 1804–1808.
[26] J. G. Proakis and M. Salehi, *Digital Communications*, 5th ed. New York, NY, USA: McGraw-Hill, 2014.
[27] A. F. Molisch, *Wireless Communications*. New York, NY, USA: Wiley, 2011.

[28] G. Caire and S. Shamai (Shitz), "On the achievable throughput of a multiantenna Gaussian broadcast channel," *IEEE Trans. Inf. Theory*, vol. 49, no. 7, pp. 1691–1706, Jul. 2003.
[29] S. Vishwanath, N. Jindal, and A. Goldsmith, "Duality, achievable rates, and sum-rate capacity of Gaussian MIMO broadcast channels," *IEEE Trans. Inf. Theory*, vol. 49, no. 10, pp. 2658–2668, Oct. 2003.
[30] P. Viswanath and D. N. C. Tse, "Sum capacity of the vector Gaussian broadcast channel and uplink-downlink duality," *IEEE Trans. Inf. Theory*, vol. 49, no. 8, pp. 1912–1921, Aug. 2003.
[31] W. Yu and J. M. Cioffi, "Sum capacity of Gaussian vector broadcast channels," *IEEE Trans. Inf. Theory*, vol. 50, no. 9, pp. 1875–1892, Sep. 2002.
[32] M. H. M. Costa, "Writing on dirty paper," *IEEE Trans. Inf. Theory*, vol. IT-29, no. 3, pp. 439–441, May 1983.
[33] N. Jindal, W. Rhee, S. Vishwanath, S. A. Jafar, and A. Goldsmith, "Sum power iterative water-filling for multi-antenna Gaussian broadcast channels," *IEEE Trans. Inf. Theory*, vol. 51, no. 4, pp. 1570–1580, Apr. 2005.
[34] P. He and L. Zhao, "Correction of convergence proof for iterative water-filling in Gaussian MIMO broadcast channels," *IEEE Trans. Inf. Theory*, vol. 57, no. 4, pp. 2539–2543, Apr. 2011.
[35] A. Paulraj, R. Nabar, and D. Gore, *Introduction to Space-Time Wireless Communications*, 1st ed. Cambridge, U.K.: Cambridge Univ. Press, 2008.
[36] B. Clerckx and C. Oestges, *MIMO Wireless Networks: Channels, Techniques and Standards for Multi-Antenna, Multi-User and Multi-Cell Systems*, 2nd ed. New York, NY, USA: Academic, 2013.
[37] İ. E. Telatar, "Capacity of multi-antenna Gaussian channels," *Eur. Trans. Telecommun.*, vol. 10, no. 6, pp. 585–595, 1999.
[38] E. Björnson, M. Bengtsson, and B. Ottersten, "Optimal multiuser transmit beamforming: A difficult problem with a simple solution structure [lecture notes]," *IEEE Signal Process. Mag.*, vol. 31, no. 4, pp. 142–148, Jul. 2014.
[39] A. Bourdoux *et al.*, "D1.2 MaMi channel characteristics: Measurement results," Mammoet, Utrecht, The Netherlands, Tech. Rep. ICT-619086-D1.2, Jun. 2015.
[40] F. Harrysson, J. Medbo, A. F. Molisch, A. J. Johansson, and F. Tufvesson, "Efficient experimental evaluation of a MIMO handset with user influence," *IEEE Trans. Wireless Commun.*, vol. 9, no. 2, pp. 853–863, Feb. 2010.
[41] R. S. Thomä *et al.*, "Identification of time-variant directional mobile radio channels," *IEEE Trans. Instrum. Meas.*, vol. 49, no. 2, pp. 357–364, Apr. 2000.
[42] J. Lee and N. Jindal, "Symmetric capacity of MIMO downlink channels," in *Proc. IEEE Int. Symp. Inf. Theory (ISIT)*, Seattle, WA, USA, Jul. 2096, pp. 1031–1035.
[43] P. Tejera, W. Utschick, J. A. Nossek, and G. Bauch, "Rate balancing in multiuser MIMO OFDM systems," *IEEE Trans. Commun.*, vol. 57, no. 5, pp. 1370–1380, May 2009.
[44] D. Christopoulos, S. Chatzinotas, and B. Ottersten, "Weighted fair multicast multigroup beamforming under per-antenna power constraints," *IEEE Trans. Signal Process.*, vol. 62, no. 19, pp. 5132–5142, Oct. 2014.
[45] E. Dahlman, S. Parkvall, J. Sköld, and P. Beming, *3G Evolution: HSPA and LTE for Mobile Broadband*, 2nd ed. London, U.K.: Academic, 2008.
[46] N. Cardona, *Cooperative Radio Communications for Green Smart Environments*. Gistrup, Denmark: River Publishers, 2016.
[47] B. M. Hochwald, T. L. Marzetta, and V. Tarokh, "Multiple-antenna channel hardening and its implications for rate feedback and scheduling," *IEEE Trans. Inf. Theory*, vol. 50, no. 9, pp. 1893–1909, Sep. 2004.
[48] H. Q. Ngo and E. G. Larsson, "No downlink pilots are needed in TDD massive MIMO," *IEEE Trans. Wireless Commun.*, vol. 16, no. 5, pp. 2921–2935, May 2017.
[49] A. Edelman, "Eigenvalues and condition numbers of random matrices," *SIAM J. Matrix Anal. Appl.*, vol. 9, no. 4, pp. 543–560, 1988, doi: 10.1137/0609045.
[50] T. Tao, *Topics in Random Matrix Theory*. Providence, RI, USA: AMS, 2012.
[51] G. Dartmann, X. Gong, and G. Ascheid, "Jointly optimized transmit beamforming and temporal user scheduling in multiuser multicell scenarios based on correlation knowledge," in *Proc. IEEE 33rd Sarnoff Symp.*, Princeton, NJ, USA, Apr. 2010, pp. 1–5.
[52] Z. Li, P. Li, and K. G. Shin, "MU-MIMO downlink scheduling based on users' correlation and fairness," in *Proc. IEEE 25th Int. Symp. Pers. Indoor Mobile Radio Commun. (PIMRC)*, Washington, DC, USA, Sep. 2014, pp. 407–412.
[53] T. Arai, A. Ohta, S. Kurosaki, K. Maruta, T. Iwakuni, and M. Iizika, "Correlation-based user scheduling and multi-planar parallelogram array for massive antenna systems," in *Proc. IEEE 27th Int. Symp. Pers. Indoor Mobile Radio Commun. (PIMRC)*, Valencia, Spain, Sep. 2016, pp. 1–6.
[54] S. Boyd and L. Vandenberghe, *Convex Optimization*. New York, NY, USA: Cambridge Univ. Press, 2004.

JOSE FLORDELIS received the M.S. degrees in telecommunication engineering from the Universitat Politècnica de València, Spain, and from Högskolan i Gävle, Sweden, in 2002. He is currently pursuing the Ph.D. degree with the Department of Electrical and Information Technology, Lund University, Sweden. From 2002 to 2012, he was with Ericsson, Sweden, where he contributed to the development of 3GPP LTE- and Bluetooth-based solutions. His main research interests are measurement, characterization, and modelling of wireless channels, especially in the areas of massive MIMO, and distributed antenna systems.

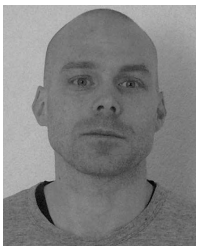

FREDRIK RUSEK was born in Lund, Sweden, in 1978. He received the M.S. and Ph.D. degrees in electrical engineering from Lund University, Sweden, in 2003 and 2007, respectively. From 2012 to 2014, he held an algorithm researcher position with Huawei, Lund. Since 2012, he held an Associate Professorship with the Department of Electrical and Information Technology, Lund Institute of Technology. His research interests include modulation theory, equalization, wireless communications, and applied information theory.

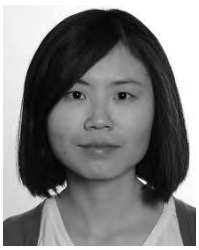

XIANG GAO received the B.S. degree in communication engineering from the University of Electronic Science and Technology of China (UESTC) in 2006 and the M.S. and Ph.D. degrees in radio communications from Lund University, Sweden, in 2010 and 2016, respectively. She was a Software Engineer at the SerComm R&D Center, Suzhou, China. She was a Wireless Communications Researcher with Facebook, Inc., CA, USA. She is currently an Associate Professor at UESTC, Chengdu, China, and is also a technical advisor for a wireless technology startup. Her current research interests are application-orientated wireless systems, including drone communications, positioning and tracking, and wireless power transfer. Her work focuses on providing solutions for wireless communication demands in future technologies.

GHASSAN DAHMAN received the Ph.D. degree from Carleton University, Ottawa, ON, Canada, in 2010. From 2010 to 2012, he was an Assistant Professor with Umm Al-Qura University, Mecca, Saudi Arabia. From 2012 to 2016, he was a Post-Doctoral Researcher with Lund University, Lund, Sweden. He is currently a Researcher with the NSERC-Ultra Electronics TCS Industrial Chair, École de Technologie Supérieure, Montreal, QC, Canada. His main research interests are radio propagation and channel modelling including: massive MIMO, distributed antenna systems, overwater point-to-point communications, and anomalous propagation of microwaves in the troposphere.

OVE EDFORS is currently a Professor in radio systems with the Department of Electrical and Information Technology, Lund University, Sweden. His research interests include statistical signal processing and low-complexity algorithms with applications in wireless communications. In the context of massive MIMO, his research focus is on how realistic propagation characteristics influence system performance and base-band processing complexity.

FREDRIK TUFVESSON received the Ph.D. degree from Lund University, Sweden, in 2000. After two years at a startup company, he joined the Department of Electrical and Information Technology, Lund University, where he is currently a Professor of radio systems. His main research interests are channel modelling, measurements and characterization for wireless communication, with applications in various areas such as massive MIMO, UWB, mm wave communication, distributed antenna systems, radio-based positioning, and vehicular communication. He has authored around 60 journal papers and 120 conference papers. He received the Neal Shepherd Memorial Award for the Best Propagation Paper in the IEEE TRANSACTIONS ON VEHICULAR TECHNOLOGY.